# USP7 regulates ALS-associated proteotoxicity and quality control through the NEDD4L–SMAD pathway

Tao Zhang[a,b,1], Goran Periz[a,b,1], Yu-Ning Lu[a,b], and Jiou Wang[a,b,2]

[a]Department of Biochemistry and Molecular Biology, Johns Hopkins Bloomberg School of Public Health, Johns Hopkins University, Baltimore, MD 21205; and [b]Department of Neuroscience, Johns Hopkins University School of Medicine, Baltimore, MD 21205

Edited by H. Robert Horvitz, Massachusetts Institute of Technology, Cambridge, MA, and approved October 5, 2020 (received for review July 9, 2020)

**An imbalance in cellular homeostasis occurring as a result of protein misfolding and aggregation contributes to the pathogeneses of neurodegenerative diseases, including amyotrophic lateral sclerosis (ALS). Here, we report the identification of a ubiquitin-specific protease, USP7, as a regulatory switch in a protein quality-control system that defends against proteotoxicity. A genome-wide screen in a *Caenorhabditis elegans* model of SOD1-linked ALS identified the USP7 ortholog as a suppressor of proteotoxicity in the nervous system. The actions of USP7 orthologs on misfolded proteins were found to be conserved in *Drosophila* and mammalian cells. USP7 acts on protein quality control through the SMAD2 transcription modulator of the transforming growth factor β pathway, which activates autophagy and enhances the clearance of misfolded proteins. USP7 deubiquitinates the E3 ubiquitin ligase NEDD4L, which mediates the degradation of SMAD2. Inhibition of USP7 protected against proteotoxicity in mammalian neurons, and SMAD2 was found to be dysregulated in the nervous systems of ALS patients. These findings reveal a regulatory pathway of protein quality control that is implicated in the proteotoxicity-associated neurodegenerative diseases.**

protein misfolding | USP7 | NEDD4L | SMAD | protein quality control

The proteome maintains its homeostasis to allow cells to survive various challenges, from internal errors to environmental stresses. Failure to maintain homeostasis can lead to the accumulation of misfolded proteins and therefore proteotoxicity that damages cells. To counteract proteotoxicity, organisms have evolved elaborate protein quality-control systems that are essential for clearing misfolded and aggregated proteins; these systems include molecular chaperones, the ubiquitin–proteasome system, and autophagy (1–3). Breakdown of protein quality control and accumulation of toxic misfolded and aggregated proteins is a common theme shared by many degenerative diseases of the nervous system, including Creutzfeldt–Jakob's, Alzheimer's, Parkinson's, and Huntington's diseases; frontotemporal dementia (FTD); and amyotrophic lateral sclerosis (ALS) (4). Consequently, understanding the pathways and regulation of protein quality-control mechanisms can shed light on basic cell biology and suggest approaches to alleviate proteotoxicity and neurodegeneration (5).

ALS is characterized by progressive motor neuron loss that leads to eventual muscular atrophy, paralysis, and respiratory failure (6). Mutations in Cu/Zn superoxide dismutase (SOD1) were the first discovered genetic cause of ALS (7). Although the wild-type (WT) form of the SOD1 protein ($SOD1^{WT}$) has a highly stable Greek key β-barrel structure (8), its mutant proteins bearing disease-linked mutations exhibit a heightened propensity to misfold and aggregate and have been used as a reliable molecular model for studying proteotoxicity (9–11). Recently, mutations in several other genes, including TAR DNA-binding protein (TDP-43), have been linked to ALS (12). The proteinaceous inclusions containing WT TDP-43 are a pathological hallmark of a variety of neurodegenerative diseases, such as the majority of ALS, nearly half of FTD, and a subset of Alzheimer's disease cases (13, 14). Unlike SOD1 showing distinct disparity between the WT and mutant proteins in their biochemical and toxic features, the WT form of TDP-43 protein, an RNA-binding protein with a low-complexity domain, is itself prone to aggregate when mislocalized under both normal stress and pathological conditions and can be used as another molecular model for studying the regulation of proteotoxicity (15, 16).

Although proteotoxicity is known to be counteracted by quality-control systems, how these systems are regulated in a coordinated manner to mount an effective defense against proteotoxic stress is complicated. For example, one such regulatory switch involves the activation of the heat shock factor 1 (HSF1) transcription factor in response to heat or proteotoxic stress, which is followed by HSF1's promotion of molecular chaperone expression to enhance protein quality control (17). A multitude of regulatory systems likely exist for protein quality control, but most have yet to be elucidated.

Simple organisms such as *Caenorhabditis elegans* offer tractable systems for uncovering key players in the complex regulation of protein homeostasis through unbiased screening studies. Using *C. elegans* genetic screens for potent suppressors of proteotoxicity, we have identified ubiquitination factor E4B (UBE4B) and lysine-specific demethylase (LSD1) as members of a conserved regulatory pathway (18). Additional screens have led to the identification of two more members of this regulatory pathway,

## Significance

**Protein homeostasis is fundamental to the functioning of all living cells. Perturbation of the homeostasis, or proteotoxicity, plays an important role in the pathogenesis of amyotrophic lateral sclerosis and related neurodegenerative diseases. To guard against proteotoxicity, cells have evolved sophisticated quality-control mechanisms that make adaptations including enhanced turnover of misfolded proteins. However, how the quality-control systems are coordinated through higher-order regulatory pathways is not fully understood. We have discovered a unique suppressor of proteotoxicity, the ubiquitin-specific protease USP7, whose action is conserved from invertebrate to mammalian systems and mediated by a substrate cascade involving NEDD4L and SMAD2. These findings reveal a previously unknown regulatory pathway for protein quality control and provide new strategies for developing interventions for neurodegenerative diseases.**

Author contributions: T.Z., G.P., Y.-N.L., and J.W. designed research; T.Z., G.P., Y.-N.L., and J.W. performed research; T.Z., G.P., Y.-N.L., and J.W. analyzed data; T.Z., G.P., and J.W. wrote the paper; and J.W. supervised the project.

The authors declare no competing interest.

This article is a PNAS Direct Submission.



[1]T.Z. and G.P. contributed equally to this work.

[2]To whom correspondence may be addressed. Email: jiouw@jhu.edu.

This article contains supporting information online at https://www.pnas.org/lookup/suppl/doi:10.1073/pnas.2014349117/-/DCSupplemental.

First published October 26, 2020.

Lethal(3)malignant brain tumor-like protein 1 (L3MBTL1) and SET domain-containing protein 8 (SETD8) (19). These genes modify proteotoxicity through a p53-dependent transcriptional program that regulates the expression of the protein quality-control machinery. The activation of p53-mediated transcription in response to protein misfolding stress is distinct from HSF1-mediated transcription (20). The exquisite regulation of protein homeostasis in the cell suggests that there are even more regulatory switches and pathways.

Modification of protein substrates by ubiquitination is a principal mechanism that serves to mark proteins for degradation (21). Ubiquitination is a process driven by reactions catalyzed by a series of enzymes, including ubiquitin-activating enzymes (E1), ubiquitin-conjugating enzymes (E2), and ubiquitin ligases (E3), that covalently add ubiquitin at the lysine residue of a substrate protein. E3 ubiquitin ligases are considered to be primarily responsible for the substrate specificity of the ubiquitination modification (22). Ubiquitination is a reversible process, and in mammals there are more than 90 deubiquitinases, enzymes that are capable of removing ubiquitin from ubiquitinated proteins (23). The largest class of deubiquitinases is a family of cysteine proteases known as ubiquitin-specific peptidases (USPs), with more than 50 family members in humans. Ubiquitin plays a role in many cellular processes, and deubiquitinases are also thought to participate in diverse cellular functions by regulating the stability and activity of their substrates (23). Deubiquitinases can act directly on the core machinery for protein quality control; for example, the proteasome-associated deubiquitinase USP14 or its homolog has been shown to remove ubiquitin chains from proteasomal substrates and allosterically modulate proteasomal activity (24, 25). However, whether deubiquitinases participate in the higher-order regulation of protein quality control remains to be elucidated.

Here we report the identification of USP7 as a conserved regulator of protein quality control that influences the turnover of the ALS-associated proteins SOD1 and TDP-43. We found that the TGFβ–SMAD pathway is involved in protein quality control and mediates the effect of USP7 on the clearance of misfolded proteins. USP7 deubiquitinates NEDD4L, the E3 ligase for SMAD2, and influences the SMAD-mediated transcriptional activity that promotes protein quality control. SMAD2 proteins are up-regulated in ALS patients' tissues, suggesting that this pathway of protein quality control may be involved in the pathophysiology of neurodegenerative diseases.

## Results

**Loss of *Math-33* Suppresses Proteotoxicity Induced by SOD1$^{G85R}$ in *C. elegans*.** To search for new players involved in regulating proteotoxicity in the intact nervous system, we employed *C. elegans* stably expressing human SOD1 with the ALS-linked mutation G85R under the pan-neuronal *snb-1* promoter. In this transgenic worm, the expression of SOD1$^{G85R}$ leads to neurotoxicity and impaired locomotion, which are not seen in control strains expressing the WT SOD1$^{WT}$ transgene (26). The SOD1$^{G85R}$ protein is highly prone to misfolding and, when tagged with yellow fluorescent protein (YFP), produces microscopically visible fluorescent aggregates in the neurons of *C. elegans*. Using this *C. elegans* model as a tractable system for investigating proteotoxicity and neurodegeneration, we performed a genome-wide RNA interference (RNAi) screen on an enhanced RNAi background of *eri-1(mg366);lin-15B(n744)* to identify modifiers of SOD1$^{G85R}$ protein aggregates (26). This screen was performed by feeding the SOD1$^{G85R}$-YFP *C. elegans* with individual clones of a library of *Escherichia coli* expressing double-stranded RNAs (dsRNAs) (27). While a number of genes whose inactivation increased SOD1$^{G85R}$-YFP aggregation were identified (26), we also searched for suppressors that showed reduced protein aggregation based on the brightness and size of the fluorescent SOD1$^{G85R}$-YFP aggregates (*SI Appendix*, Fig. S1*A*). In general, most of the RNAi with a substantial reduction in the fluorescent intensity of the SOD1$^{G85R}$-YFP aggregates showed severe defects in development and viability (*SI Appendix*, Table S1), suggesting that processes essential for cellular fitness such as translation had been affected, and these RNAi clones were excluded from further study. One unique suppressor, conferred by the dsRNAs against *math-33*, the *C. elegans* ortholog of USP7 (Fig. 1*A*), led to a considerable reduction in the fluorescence of SOD1$^{G85R}$-YFP aggregates without a severe developmental or viability defect and was selected for further analysis.

To verify that *math-33* is a suppressor of the screened phenotype, we obtained mutant *C. elegans* carrying a loss-of-function allele, *math-33(ok2974)*, which removes 458 base pairs from the *math-33* gene, resulting in a truncated protein containing the first 445 amino acids of the MATH-33 protein, followed by a stretch of 40 amino acids before reaching a stop codon (Fig. 1*A*). In accordance with previously described loss-of-function phenotypes (28), the *math-33(ok2974)* mutant showed incomplete embryonic lethality that contributes to a smaller size of offspring population than that of WT *C. elegans* (*SI Appendix*, Fig. S1*B*). However, the *math-33(ok2974)* mutant has a normal lifespan at 20 °C compared to that of WT *C. elegans* (*SI Appendix*, Fig. S1*C*). Importantly, after *math-33(ok2974)* was crossed into the SOD1$^{G85R}$-YFP strain, the fluorescent intensity of SOD1$^{G85R}$-YFP aggregates in the neurons was significantly lower than that in worms carrying SOD1$^{G85R}$-YFP(*iwls8*) on the WT background (Fig. 1*B*). Next, we examined the levels of soluble and insoluble SOD1$^{G85R}$-YFP in the *C. elegans* strains with or without the loss of *math-33*. *C. elegans* lysates were subjected to detergent extraction and high-speed centrifugation to separate the supernatant fraction, which contains the soluble and small oligomers of SOD1$^{G85R}$-YFP protein, from the insoluble pellet fraction, which contains SOD1$^{G85R}$-YFP aggregates of sufficient size to be sedimented in the assay, as described previously (26). As shown by immunoblot analysis, the SOD1$^{G85R}$-YFP protein levels in both the supernatant and pellet fractions were significantly decreased in SOD1$^{G85R}$-YFP(*iwls8*);*math-33(ok2974)* worms, as compared to those in worms carrying SOD1$^{G85R}$-YFP(*iwls8*) alone (Fig. 1*C*). Notably, the mRNA level of SOD1$^{G85R}$-YFP was not changed between the worms with or without *math-33(ok2974)*, suggesting that the effect of the loss of *math-33* on SOD1$^{G85R}$-YFP levels occurred at the protein level (Fig. 1*D*). We then asked how the loss of *math-33* affected the impaired locomotion caused by the expression of SOD1$^{G85R}$-YFP in neurons. Consistent with the concept that misfolded SOD1$^{G85R}$-YFP is toxic to neurons, SOD1$^{G85R}$-YFP(*iwls8*);*math-33(ok2974)* worms, which have reduced levels of mutant SOD1 protein, showed a significant lessening of the locomotor defects when compared to worms carrying SOD1$^{G85R}$-YFP(*iwls8*) on the WT background, as measured by the thrashing rate of developmentally synchronized worms in liquid M9 buffer (Fig. 1*E*). To test whether loss of *math-33* affects the level of transgenic SOD1$^{WT}$-YFP protein that is in the soluble form (26), we crossed *math-33(ok2974)* into the SOD1$^{WT}$-YFP strain and observed no significant change in the protein level of SOD1$^{WT}$-YFP (*SI Appendix*, Fig. S1*D*). These data demonstrate that the loss of *math-33* is sufficient to reduce both the level of misfolded mutant SOD1 protein and its neurotoxicity in *C. elegans*.

**Loss of USP7 Enhances Clearance of Misfolded Proteins in Mammalian Cells.** *C. elegans math-33* is orthologous to human USP7, sharing similar protein domains and being conserved among many species (Fig. 1*A* and *SI Appendix*, Fig. S1*E*). To determine whether the modulation of USP7 influences the level of misfolded proteins in mammalian cells, we utilized a cell-based assay to quantify the solubility of the SOD1$^{G85R}$ protein. As in the *C.*

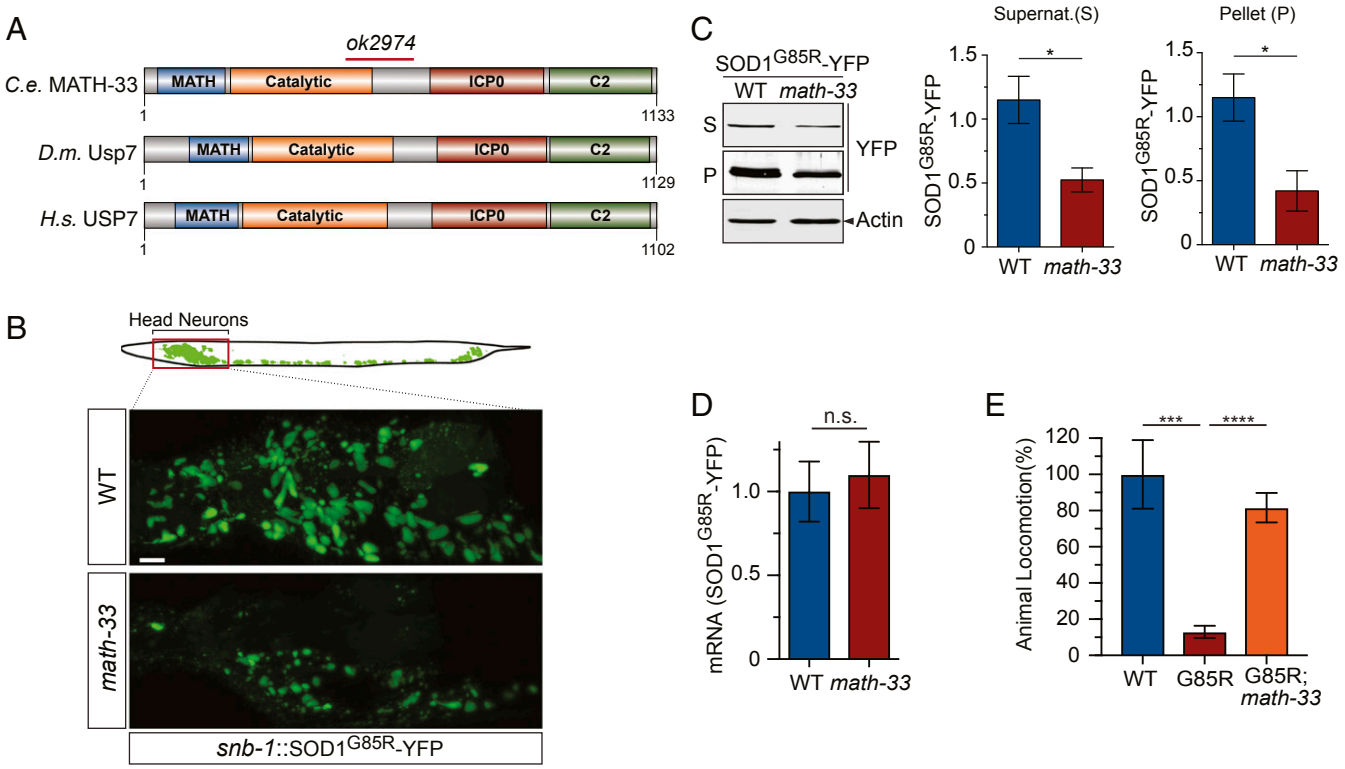


**Fig. 1.** An RNAi screen for suppressors of aggregation of mutated SOD1$^{G85R}$-YFP in *C. elegans* identifies *math-33* as a strong suppressor of aggregation. (*A*) *C. elegans* MATH-33 and its homologs in *Drosophila* and human, Usp7 and USP7, respectively, share all major protein domains. These include the Meprin And Traf Homology domain (MATH), catalytic peptidase domain, herpes simplex virus ICP0 protein binding domain (ICP0), and C2 terminal domain. The position of a deletion mutation, *ok2974*, in the *C. elegans* mutant is indicated with a red bar. (*B*) The *math-33(ok2974)* mutant worms showed reduced aggregation of SOD1$^{G85R}$-YFP, as evidenced by the reduced fluorescent signal in head neurons when compared to the controls on the WT background. (Scale bar, 5 μm.) (*C*) Western blot analysis of soluble (S) and pellet (P) protein fractions from the WT and *math-33(ok2974)* mutant worms. Representative immunoblots of SOD1$^{G85R}$-YFP (*Left*) and quantification of SOD1$^{G85R}$-YFP protein from the S (*Middle*; *$P < 0.05$) and P (*Right*; *$P < 0.05$) fractions are shown ($n = 3$). (*D*) qRT-PCR analysis of the mRNA expression levels of the SOD1$^{G85R}$ transgene in *math-33(ok2974)* mutant *C. elegans* as compared to the control background (WT) ($n = 3$; n.s., nonsignificant). (*E*) Locomotor behavior, as measured by the thrashing assay, of *C. elegans* with neuronal expression of SOD1$^{G85R}$, with or without the suppressor mutation *math-33(ok2974)*, as compared to control *C. elegans* expressing SOD1$^{WT}$ ($n = 9$; ***$P < 0.001$, ****$P < 0.0001$). Error bars indicate ± SEM.

*elegans* protein solubility assay described above, HEK293 cells expressing SOD1$^{G85R}$ were subjected to detergent extraction and high-speed centrifugation to separate the soluble SOD1 proteins to the supernatant and the insoluble aggregated SOD1$^{G85R}$ to the pellet fraction, which were then analyzed by immunoblotting. Consistent with the observation that SOD1$^{G85R}$ is highly prone to misfolding and aggregation, the mutant protein was found in both the supernatant and pellet, whereas the endogenous SOD1$^{WT}$ protein, expressed at a level comparable to that of SOD1$^{G85R}$, was found only in the supernatant (Fig. 2*A*), indicating that the mutant but not the WT protein formed aggregates in the cells. The WT and mutant proteins could be distinguished by the fact that SOD1$^{G85R}$ migrates faster than does SOD1$^{WT}$ on sodium dodecyl sulfate polyacrylamide gel electrophoresis (SDS-PAGE) gels (29). Notably, when USP7 was knocked down with its specific small hairpin RNAs (shRNAs), the levels of SOD1$^{G85R}$ protein were decreased in both the supernatant and pellet fractions, whereas the levels of endogenous SOD1$^{WT}$ protein were unchanged (Fig. 2*A*). Quantification of the immunoblot analysis confirmed the significant decrease in SOD1$^{G85R}$ protein in both the soluble and insoluble aggregated forms in the presence of USP7-specific shRNAs, as compared to the nontargeting shRNA control (Fig. 2*A*). Moreover, the knockdown of USP7 had no effect on the levels of exogenously expressed SOD1$^{WT}$ protein (*SI Appendix*, Fig. S2*A*), confirming that the effect was specific to the misfolded SOD1$^{G85R}$ protein but not to the well-folded SOD1$^{WT}$ protein. We then asked whether the activity of USP7 is required for this phenotype by using a small-molecule inhibitor of USP7, HBX41108 (30), analyzing the levels of WT or mutant SOD1 protein after treating HEK293 cells with the inhibitor. Treatment with HBX41108 led to a significant, dose-dependent decrease in the levels of misfolded SOD1$^{G85R}$ protein but had no effect on endogenous SOD1$^{WT}$ protein (Fig. 2*B*). Moreover, the treatment of HBX41108 had no effect on the levels of exogenously expressed SOD1$^{WT}$ protein (*SI Appendix*, Fig. S2*B*), confirming that loss of USP7 activity specifically led to the reduction of misfolded SOD1 protein.

Next, we asked whether USP7 regulates the turnover of the SOD1$^{G85R}$ protein. We performed a cycloheximide chase experiment to measure the half-life of SOD1$^{G85R}$, with or without the knockdown of USP7. Once new protein synthesis had been blocked with cycloheximide, we lysed the HEK293 cells expressing SOD1$^{G85R}$ at different time points and analyzed the SOD1$^{G85R}$ protein levels by immunoblotting. The knockdown of USP7 significantly decreased the half-life of the SOD1$^{G85R}$ protein, as compared to the control shRNA treatment, indicating that a loss of USP7 promotes the degradation of the SOD1$^{G85R}$ protein (Fig. 2*C*). Notably, the turnover rate of the SOD1$^{WT}$ protein, expressed at a level comparable to that of SOD1$^{G85R}$, was not affected by the knockdown of USP7, suggesting that the

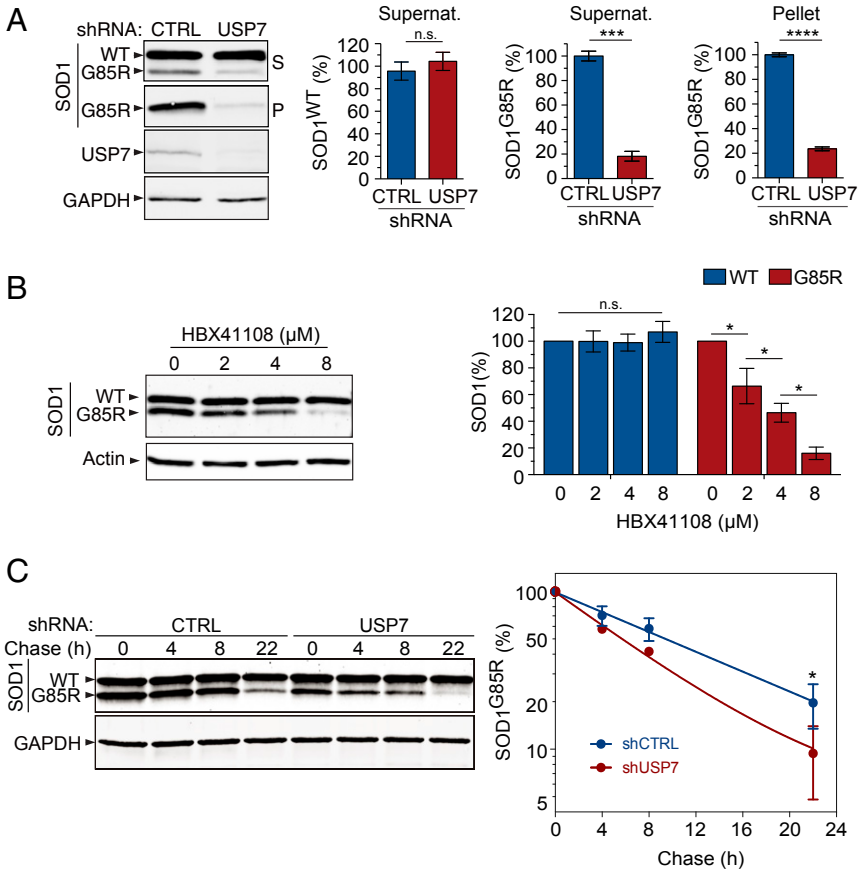


**Fig. 2.** A reduction in the USP7 function increases clearance of misfolded proteins. (*A*) Western blot analysis of cell lysates derived from mock (CTRL) or USP7 knockdown in HEK293 cells expressing $SOD1^{G85R}$. USP7 knockdown reduced the $SOD1^{G85R}$ proteins in both the supernatant (S) and pellet (P) fractions, without affecting the level of endogenous WT SOD1 ($SOD1^{WT}$). Quantification of $SOD1^{WT}$ and $SOD1^{G85R}$ protein levels by immunoblotting is shown ($n = 3$; $^{***}P < 0.001$, $^{****}P < 0.0001$; n.s., nonsignificant). (*B*) A small-molecule inhibitor of USP7, HBX41108, reduced the level of misfolded $SOD1^{G85R}$ protein, but not that of $SOD1^{WT}$ protein in HEK293 cells. A dose-dependent effect on the level of $SOD1^{G85R}$ protein with increasing concentrations of HBX41108, as compared to the vehicle control (DMSO), was observed in the supernatants of the cell lysates ($n = 3$; n.s., nonsignificant; $^{*}P < 0.05$). (*C*) Western blots of a representative cycloheximide chase experiment to determine the SOD1 protein half-life in the USP7 knockdown cells versus controls (*Left*). Quantification of the $SOD1^{G85R}$ clearance as analyzed by immunoblotting is shown (*Right*). The graph indicates the relative band intensity of $SOD1^{G85R}$ at each chase time point in the USP7 knockdown cells versus controls ($n = 3$; *overall $P < 0.05$ for the three time points after 0 h). Error bars indicate ± SEM.

effect of USP7 on the protein turnover is specific to misfolded mutant proteins (*SI Appendix*, Fig. S2*C*).

To determine whether the effect of USP7 on the protein level is specific to SOD1, we examined the solubility of another disease-linked mutant protein, $TDP\text{-}43^{Q331K}$, with or without USP7 knockdown. As in the SOD1 solubility assay, HEK293 cells expressing $TDP\text{-}43^{Q331K}$ were subjected to detergent extraction and high-speed sedimentation to separate the supernatant and pellet fractions. The knockdown of USP7 significantly decreased the levels of $TDP\text{-}43^{Q331K}$ in both the supernatant and pellet fractions, as compared to the nontargeting shRNA control (*SI Appendix*, Fig. S2*D*). Unlike SOD1, the WT form of TDP-43 protein is relatively unstructured and prone to misfold and aggregate and has been implicated in the majority of TDP-43 proteinopathy in ALS cases. Consistently, knockdown of USP7 significantly reduced the level of $TDP\text{-}43^{WT}$ protein overexpressed in HEK293 cells (*SI Appendix*, Fig. S2*E*). Taken together, these results suggest that USP7 regulates the clearance of misfolded proteins.

**USP7 Regulates Proteotoxicity via the Transforming Growth Factor β–SMAD Pathway.** To understand the downstream pathways through which USP7 regulates proteotoxicity, we performed transcriptional profiling of HEK293 cells after mock or USP7 knockdown, using microarray analysis to uncover changes in the global gene expression pattern. Then, using Ingenuity Pathway Analysis software to identify upstream regulators that are transcriptional regulators of differentially regulated genes, we found that the transforming growth factor β (TGFβ)–SMAD signaling pathway was one of the most significantly activated pathways when USP7 was knocked down, as indicated by the best Z-score ($Z = 5.07$) that the TGFβ signaling had among the top pathways analyzed (*SI Appendix*, Fig. S3). TGFβ ligands bind to receptors on the cell membrane and activate SMAD complexes, which serve as transcription factors regulating target gene expression. To test whether USP7 regulates SMAD-mediated transcriptional activity, we used a luciferase transcriptional reporter driven by a promoter under the control of copies of the SMAD-binding elements DNA sequence (31). In HEK293 cells treated with USP7-specific shRNAs, we found that the SMAD-mediated transcriptional activity was significantly increased when compared to the transcriptional activity in cells treated with control shRNAs (Fig. 3*A*). Additionally, inactivation of USP7 with the inhibitor HBX41108 also led to a significant increase in the SMAD-mediated transcriptional activity (Fig. 3*A*). Taken together,

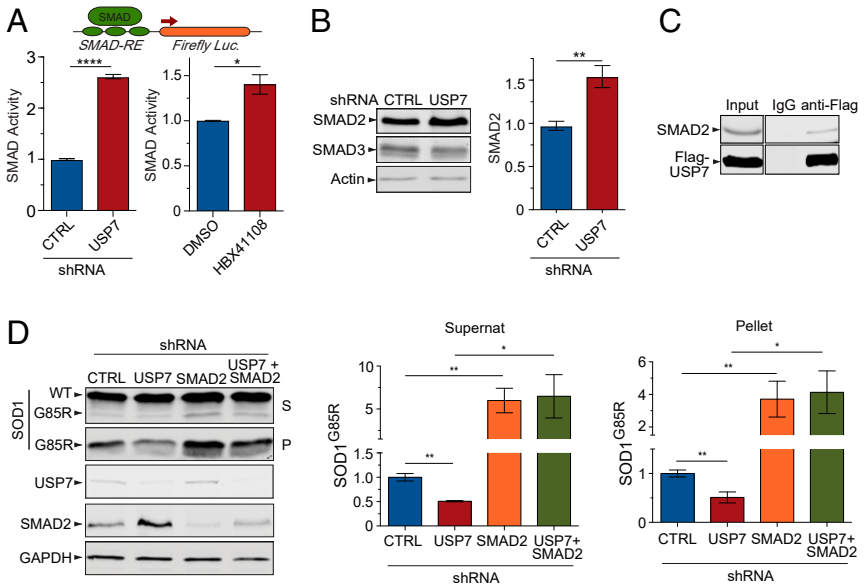


**Fig. 3.** USP7 regulates misfolded mutant SOD1 protein levels through the transcription factor SMAD2. (*A*) The SMAD transcriptional activity was increased in HEK293 cells upon USP7 knockdown (*Left*) or inhibition of USP7 by the small-molecule drug HBX41108 at 2 μM (*Right*), as measured by the SMAD response element (SMAD-RE)–mediated luciferase activity assay ($n = 3$; $^{*}P < 0.05$, $^{****}P < 0.0001$). (*B*) The protein levels of SMAD2, but not those of SMAD3, were increased upon USP7 knockdown ($n = 3$; $^{**}P < 0.01$). (*C*) Endogenous SMAD2 was coimmunoprecipitated when Flag-USP7 expressed in HEK293 cell was pulled down by the anti-Flag antibody but not the IgG control. (*D*) Immunoblot analysis of $SOD1^{G85R}$ in cells with USP7 or SMAD2 knockdown, or double knockdown, indicated that loss of SMAD2 abolished the effect of USP7 on the regulation of $SOD1^{G85R}$ levels in both the supernatant and pellet fractions ($n = 4$; $^{*}P < 0.05$, $^{**}P < 0.01$). Error bars indicate ± SEM.

these results indicate that USP7 is a negative regulator of SMAD-mediated transcriptional activity.

Next, we asked if there was any change in the abundance of the SMAD proteins that would correspond to the activation of the pathway triggered by the loss of USP7. We used immunoblot analysis to measure the levels of major SMAD proteins, including SMAD2 and SMAD3, in HEK293 cells after knockdown of USP7. Whereas we saw no change in SMAD3 after the knockdown, we found a significant increase in the levels of SMAD2 protein in the cells treated with USP7-specific shRNAs, as compared to those from control shRNA-treated cells (Fig. 3*B*). Next, we asked whether USP7 is physically associated with SMAD2. In HEK293 cells expressing Flag-tagged USP7, an anti-Flag antibody pulled down the tagged USP7 together with coimmunoprecipitated endogenous SMAD2, whereas a control immunoglobulin G (IgG) antibody failed to pull down either Flag-USP7 or SMAD2 (Fig. 3*C*). These results suggest that USP7 is biochemically associated with SMAD2 and may regulate the stability of SMAD2 at the protein level.

To determine whether the TGFβ–SMAD pathway plays a role in the regulation of proteotoxicity, we performed protein solubility assays to ask whether the TGFβ ligand can induce changes in the solubility of the $SOD1^{G85R}$ protein. HEK293 cells expressing $SOD1^{G85R}$ were treated with TGFβ at various concentrations, and the levels of $SOD1^{G85R}$ protein in both the supernatant and pellet fractions of the cell lysates were quantified by immunoblotting. We found that the TGFβ treatment produced a concentration-dependent decrease in the amount of insoluble $SOD1^{G85R}$ in the pellet fractions, suggesting that the TGFβ–SMAD pathway alone is sufficient to reduce the accumulation of misfolded $SOD1^{G85R}$ proteins (*SI Appendix*, Fig. S2*F*).

To further confirm a role for the TGFβ–SMAD pathway in the regulation of proteotoxicity by USP7, we asked whether ablating the SMAD transcription factor would affect the regulation of $SOD1^{G85R}$ levels by USP7. Since SMAD2 is up-regulated by USP7 removal, we used the protein solubility assay to assess the role of SMAD2 by knocking it down, alone or together with USP7. Consistent with the concept that the TGFβ–SMAD pathway positively regulates the clearance of misfolded $SOD1^{G85R}$ proteins, knockdown of SMAD2 led to an increased accumulation of $SOD1^{G85R}$ in the insoluble fractions from HEK293 cells expressing the mutant protein (Fig. 3*D*). Importantly, in the cells treated with double knockdown of SMAD2 and USP7, the loss of SMAD2 was sufficient to reverse the reduction in insoluble $SOD1^{G85R}$ in the pellet fractions that was induced by USP7 knockdown (Fig. 3*D*). Moreover, we analyzed the levels of endogenous $SOD1^{WT}$ protein and found no evidence that USP7 or SMAD2 regulated the level of WT SOD1 protein (*SI Appendix*, Fig. S2*G*). These data suggest that SMAD2 is required as an effector downstream of USP7 in the regulation of mutant $SOD1^{G85R}$ protein clearance.

**USP7 Modulates the Ubiquitination of NEDD4L, the E3 Ligase of SMAD2.** Since deubiquitination of protein substrates typically leads to their escape from degradation, and loss of USP7 increases the level of SMAD2, we reasoned that USP7 may deubiquitinate a negative regulator of SMAD2 such as NEDD4L, an E3 ubiquitin ligase that has been shown to target SMAD proteins and limit TGFβ signaling (32). To determine whether NEDD4L mediates the regulatory effect of USP7 on SMAD2, we used immunoblotting to examine the level of NEDD4L after knockdown of USP7 in HEK293 cells and found that a loss of USP7 significantly decreased the level of the NEDD4L protein (Fig. 4*A*). Furthermore, inactivation of USP7 with the inhibitor HBX41108 also decreased the level of NEDD4L protein (*SI Appendix*, Fig. S2*H*). To determine whether NEDD4L is a potential substrate of USP7, we asked whether there was a physical interaction between these two proteins. After HEK293 cells were transfected to express Flag-tagged USP7, the coimmunoprecipitation analysis showed that endogenous NEDD4L was pulled down by anti-Flag antibody but not a control IgG, indicating that USP7 is biochemically associated with NEDD4L (Fig. 4*B*).

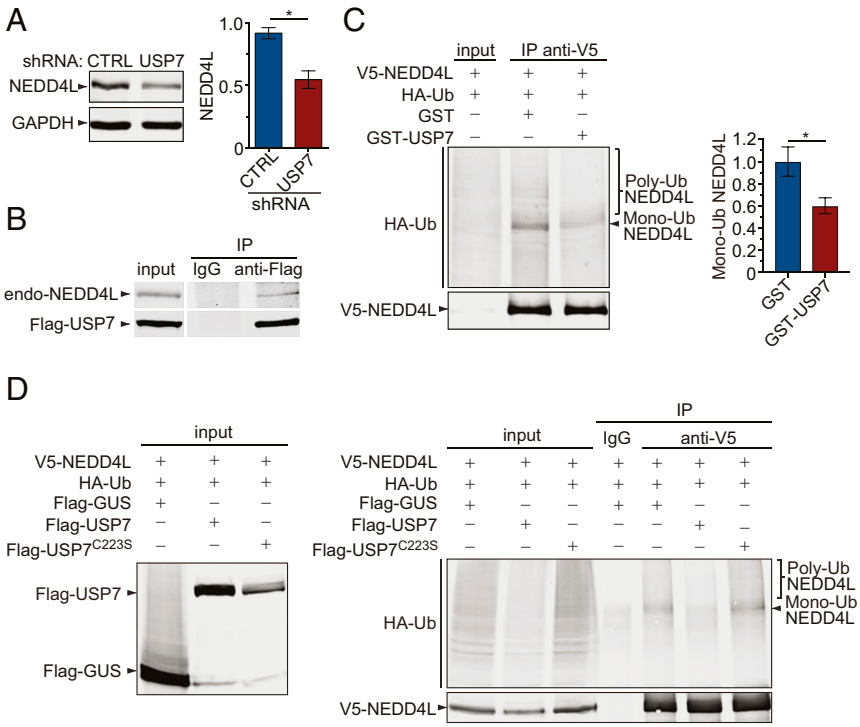


**Fig. 4.** USP7 deubiquitinates NEDD4L, the E3 ligase for SMAD2. (*A*) Immunoblots and quantification of endogenous NEDD4L in HEK293 cells with USP7 or control knockdown ($n = 3$; $^*P < 0.05$). (*B*) Endogenous NEDD4L was coimmunoprecipitated when Flag-USP7 expressed in HEK293 cells was pulled down by the anti-Flag antibody but not the IgG control. (*C*) In the in vitro deubiquitination assay, V5-NEDD4L expressed in HEK293 cells was immunoprecipitated and used as a substrate for incubation with purified GST-USP7 or GST. The presence of USP7 significantly decreased the levels of ubiquitinated NEDD4L protein ($n = 3$; $^*P < 0.05$). Error bars indicate ± SEM. (*D*) In the in vivo deubiquitination assay, cell lysates expressing Flag-USP7 variants, V5-NEDD4L, and HA-Ub and were incubated with anti-V5 antibody to pull down NEDD4L, and the immunoprecipitates were subjected to analysis of ubiquitination by immunoblotting. C223S is a catalytic mutant of USP7, and GUS is a control.

Next, we performed both in vitro and cell-based deubiquitination assays to address whether NEDD4L is a substrate of USP7. In an in vitro deubiquitination assay, the ubiquitinated V5-NEDD4L was immunoprecipitated from HEK293 cells expressing the protein and incubated with purified recombinant GST-USP7 protein, or GST as a control, in a deubiquitination reaction buffer. The recombinant GST-USP7 exhibited deubiquitinase activity on V5-NEDD4L in the in vitro assay, since examination of the status of ubiquitination of V5-NEDD4L revealed a significantly lower level of ubiquitinated V5-NEDD4L proteins in the presence of GST-USP7 than in the presence of the GST control (Fig. 4*C*). Therefore, these results establish that NEDD4L is a direct substrate of USP7.

In a cell-based assay, recombinant NEDD4L, USP7, and ubiquitin, each fused with a distinct polypeptide tag, were expressed in HEK293 cells, and the ubiquitination status of NEDD4L was analyzed by immunoprecipitation of the substrate protein, followed by immunoblotting with anti-ubiquitin antibodies. The expression of Flag-tagged USP7, but not control Flag-tagged β-glucuronidase (GUS), resulted in significantly decreased ubiquitination of V5-NEDD4L (Fig. 4*D*), consistent with the idea that USP7 deubiquitinates NEDD4L. Notably, the replacement of WT USP7 with its catalytically inactive mutant, C223S (33), abolished the effects on the ubiquitination of V5-NEDD4L in this assay, confirming that the enzymatic activity of USP7 is required for the deubiquitination of NEDD4L (Fig. 4*C*).

**The USP7–SMAD2 Pathway Regulates Proteotoxicity through Autophagy.** Given our observation that SMAD2 mediates the regulation of proteotoxicity by USP7 (Fig. 3*D*), we sought to identify the mechanisms through which the USP7–SMAD2 pathway acts. Since previous studies reported that TGFβ is a negative regulator of the proteasome but a positive regulator of autophagy (34, 35) and we also observed that SMAD2 negatively regulates the proteasomal activity (*SI Appendix*, Fig. S4 *A* and *B*), we focused on autophagy as the candidate mechanism through which the SMAD2-mediated pathway promotes the degradation of misfolded proteins. We found that knockdown of SMAD2 by specific shRNAs in HEK293 cells led to a decrease in the LC3II protein (Fig. 5*A*). LC3II is a standard autophagy marker specifically localized to autophagosomes, and the lysosomal turnover of LC3II can be assayed to measure the autophagy flux. This significant reduction in LC3II protein in response to SMAD2 reduction was not altered when lysosome activity was inhibited with bafilomycin A1 (Fig. 5*A*), suggesting that the loss of SMAD2 reduces the autophagy flux in consistence with the previous reports that TGFβ positively regulates autophagy (34, 35).

Next, we examined how autophagy is regulated by USP7. In agreement with the earlier observation that the loss of USP7 enhanced the clearance of misfolded mutant SOD1 proteins, we found that USP7 knockdown increased the levels of LC3II both in the absence and presence of bafilomycin A1, suggesting that USP7 is a negative regulator of the autophagy flux (Fig. 5*B*). We also examined the effects of the USP7 inhibitor HBX41108 on LC3II levels. As in the case of the USP7 knockdown, the small-molecule inhibition of USP7 led to an increase in the levels of LC3II both in the absence and presence of bafilomycin A1 (Fig. 5*C*), consistent with the concept that the loss of USP7 positively regulates the autophagy flux.

To further examine the status of the autophagy flux, we employed a tandem fluorescent protein reporter mCherry-EGFP-LC3, which specifically labels the lysosome in red due to the preferential quenching of enhanced green fluorescent protein (EGFP) over

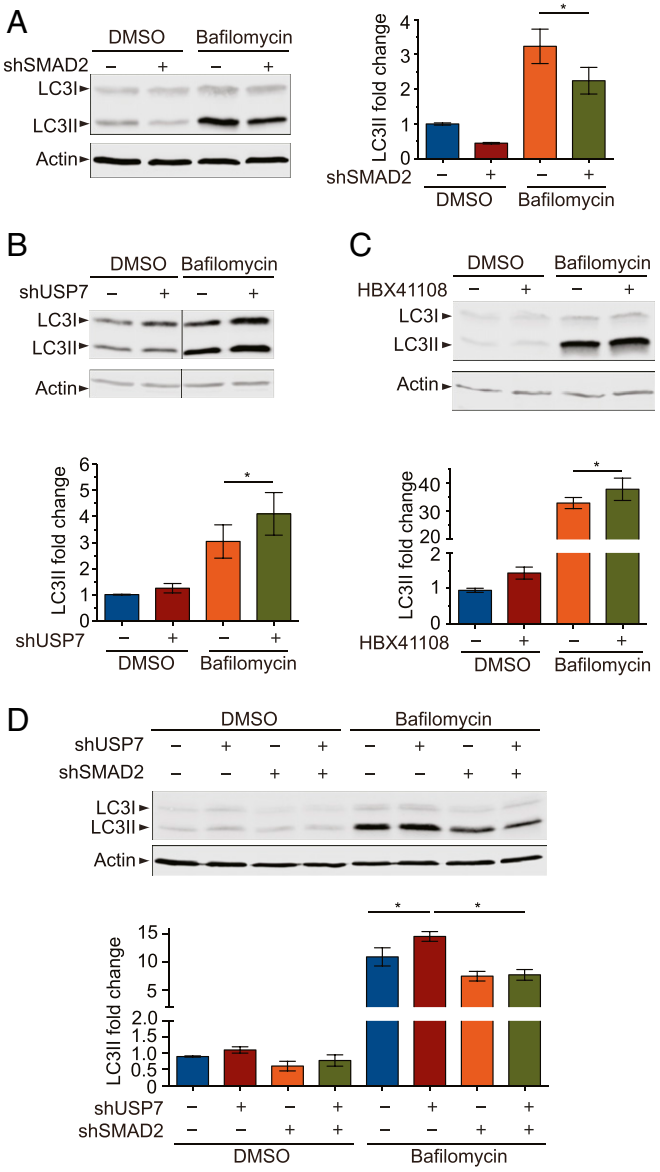


**Fig. 5.** USP7 regulates autophagy through SMAD2. (*A*) Immunoblots of LC3II proteins in HEK293 cells after mock or SMAD2 knockdown, with or without 200 nM bafilomycin A1 treatment. Quantification of LC3II is shown ($n = 6$; $^*P < 0.05$). (*B*) Immunoblots and quantification of LC3II protein levels after mock or USP7 knockdown, with or without bafilomycin A1 treatment ($n = 8$; $^*P < 0.05$). (*C*) Immunoblots and quantification of LC3II protein levels after treatment with the USP7 inhibitor HBX41108, with or without bafilomycin A1 ($n = 6$; $^*P < 0.05$). (*D*) Immunoblots and quantification of LC3II protein levels after single or double knockdown of USP7 and SMAD2, with or without bafilomycin A1 ($n = 6$; $^*P < 0.05$). Error bars indicate ± SEM.

mCherry in the acidic environment inside the lysosome. Consistent with the immunoblot analysis of LC3II, the inhibition of USP7 with HBX41108 increased the number of red puncta in the lysosomes, suggesting an enhanced autophagic flux (*SI Appendix*, Fig. S5 *A* and *B*). Furthermore, knockdown of SMAD2 led to a significant decrease in the number of red puncta in the lysosomes, indicating that the autophagy flux was suppressed (*SI Appendix*, Fig. S5 *C* and *D*).

To further confirm the role of the USP7–SMAD2 pathway in the regulation of autophagy, we asked whether the elimination of SMAD2 would affect the activation of autophagy by USP7 knockdown. The changes in the levels of LC3II proteins induced by single knockdown of USP7 or SMAD2 were similar to those observed earlier, as measured by immunoblot analysis; however, in the cells with double knockdown of SMAD2 and USP7 the loss of SMAD2 was sufficient to reverse the increases in LC3II induced by knocking down USP7 (Fig. 5*D*), indicating that SMAD2 is required as an effector downstream of USP7 in the regulation of autophagy.

**The USP7 Ortholog Regulates Proteotoxicity in *Drosophila*.** To investigate the conserved role of USP7 in proteotoxicity in an intact nervous system of another species, we utilized a *Drosophila* model that expresses an ALS-associated human mutant $SOD1^{A4V}$ in motor neurons and develops locomotion deficits that can be measured by a climbing assay (36). Using a transgenic strain with stable RNAi-induced reduction of the *Drosophila* Usp7, the ortholog of human USP7, we found that a reduction in Usp7 in the motor neurons produced a significant rescue of the mutant SOD1-induced climbing deficits (Fig. 6*A*). Next, to determine whether the *Drosophila* ortholog of human SMAD, Smox, modulates the mutant SOD1-induced neurotoxicity, we crossed the strain showing a stable RNAi-induced reduction of Smox with the fly model expressing mutant $SOD1^{A4V}$ in motor neurons. The reduction in Smox led to significant climbing deficits in the mutant SOD1 flies (Fig. 6*A*). Since Babo in *Drosophila* is the counterpart of the TGFβ receptor that regulates downstream SMAD-like proteins (37), we also asked whether Babo regulates the proteotoxicity in the SOD1 fly model. Consistent with the fact that Babo is functionally analogous to the TGFβ receptor in *Drosophila*, knockdown of Babo

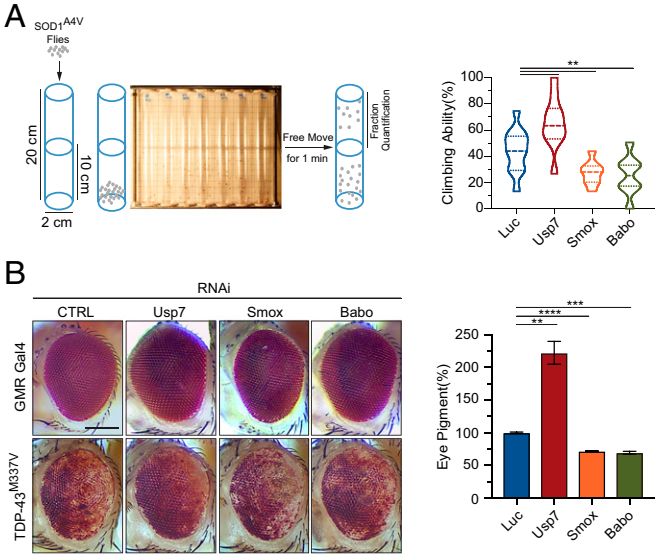


**Fig. 6.** The knockdown of *Drosophila* Usp7 suppresses neurotoxicity induced by mutant SOD1 or TDP-43. (*A*) Chart of the climbing (negative geotaxis) assay in adult *Drosophila* expressing human $SOD1^{A4V}$ in motor neurons (*Left*). Quantification of the climbing ability of *Drosophila* expressing human $SOD1^{A4V}$ in motor neurons, together with gene-specific RNAi against Usp7 (34708), Smox (26756), Babo (40866), or control RNAi (*Right*; $n = 8$ independent groups; $^{**}P < 0.01$). (*B*) Reduction in Usp7 by RNAi (34708) strongly suppresses the eye degeneration phenotypes in $TDP\text{-}43^{M337V}$ strains, while reduction in Smox (RNAi 26756) or Babo (RNAi 40866) worsens the eye degeneration phenotypes, when compared with the control Luc RNAi strain (*Left*). (Scale bar, 100 μm.) Quantification of pigment content in adult eyes confirms the protection against degeneration by a loss of Usp7 in $TDP\text{-}43^{M337V}$ strains (*Right*). The measurements represent three independent groups, each containing fly heads from two males and two females ($n = 3$; $^{**}P < 0.01$, $^{***}P < 0.001$, $^{****}P < 0.0001$). Error bars indicate ± SEM.

led to a more severe climbing deficit in the mutant SOD1 flies than did knockdown of the control shRNAs (Fig. 6*A*).

In addition, we asked how Usp7 and Smox influenced the phenotypes of transgenic *Drosophila* models expressing the ALS/FTD-related mutant protein TDP-43. As adults, flies expressing the TDP-43$^{M337V}$ mutant develop various degrees of rough eye phenotype as a result of the loss of photoreceptors and retinal degeneration (38). We asked whether the knockdown of *Drosophila* Usp7, Smox, or Babo in *Drosophila* eyes might modulate this TDP-43$^{M337V}$-induced proteotoxicity. The loss of Usp7 alleviated the neurodegeneration and loss of pigmentation in the TDP-43$^{M337V}$ fly model, but the loss of Smox or Babo resulted in a worsened eye roughness phenotype and robustly augmented the loss of pigmentation (Fig. 6*B*). Moreover, we confirmed the changes in the eye degeneration phenotypes via histological analysis of the *Drosophila* eyes using hematoxylin and eosin (H&E) staining on tissue sections. The neuronal layer in the eyes of mutant TDP-43$^{M337V}$ flies was much thinner than that of WT flies as a result of neuronal loss, and the knockdown of Usp7 alleviated the eye neurodegeneration phenotype while the knockdown of Smox or Babo worsened the eye neurodegeneration phenotype (*SI Appendix*, Fig. S6*A*).

To validate the effects of Usp7 RNAi knockdown, we generated a deletion allele of Usp7, Usp7$^{\Delta 1}$, using CRISPR editing (*SI Appendix*, Fig. S6*B*). Flies with the homozygous Usp7$^{\Delta 1}$ mutation die prematurely at the pupal stage. Flies with the heterozygous Usp7$^{\Delta 1}$ mutation developed normally and, when crossed to the SOD1$^{A4V}$ or TDP-43$^{M337V}$ flies, exhibited suppression of the climbing deficits or the eye degeneration phenotypes, respectively (*SI Appendix*, Fig. S6 *C* and *E*), confirming its protective effects. In addition, independent RNAi lines of Smox and Babo were employed to confirm the aggravated phenotypes in the SOD1$^{A4V}$ or TDP-43$^{M337V}$ flies (*SI Appendix*, Fig. S6 *C* and *E*). As a negative control, flies carrying only RNAi for Usp7, Smox or Babo, or Usp7$^{\Delta 1}$ were subjected to the climb assay and showed no alteration of their climbing ability in the control background (*SI Appendix*, Fig. S6*D*). The effects of RNAi on the expression of Usp7, Smox, and Babo were verified by quantitative reverse transcription and PCR analysis (*SI Appendix*, Fig. S6*F*). Taken together, these results suggest that the regulatory effects of the USP7–SMAD pathway on proteotoxicity-associated neurodegeneration are conserved in *Drosophila*.

**USP7-Dependent Proteotoxicity in Neurons and Dysregulation of SMAD2 in Patient Tissues.** We asked whether USP7 inhibition would alleviate proteotoxicity-induced neurotoxicity in mammalian neurons, utilizing a neurotoxicity assay employing neurons differentiated in vitro from mouse embryonic stem (mES) cells. The neurons were transduced with herpes simplex virus (HSV) expressing the human SOD1$^{WT}$ or SOD1$^{G85R}$, and their viability was assessed with the cell-permeant dye, calcein AM, which is converted to a fluorescent product inside viable neurons (39). The expression of SOD1$^{G85R}$ exerted a significant toxic effect on the neurons 2 d after transduction when compared to neurons expressing the SOD1$^{WT}$ control (Fig. 7*A*). However, the treatment with the USP7 inhibitor HBX41108 at 2 μM, a concentration well tolerated by the neurons (*SI Appendix*, Fig. S7), significantly decreased the SOD1$^{G85R}$-induced toxicity when compared to the dimethyl sulfoxide (DMSO) solvent control (Fig. 7*A*), indicating that the inhibition of USP7 protected against the toxicity of the mutant SOD1 in neurons.

To determine if the SMAD-mediated protein quality-control system is implicated in human disease mechanisms, we analyzed extracts of tissues from the spinal cords of ALS patients. When the spinal cords were examined by Western blotting for 24 ALS patients and 8 controls, we found that the level of SMAD2 protein was consistently elevated in both familial and sporadic

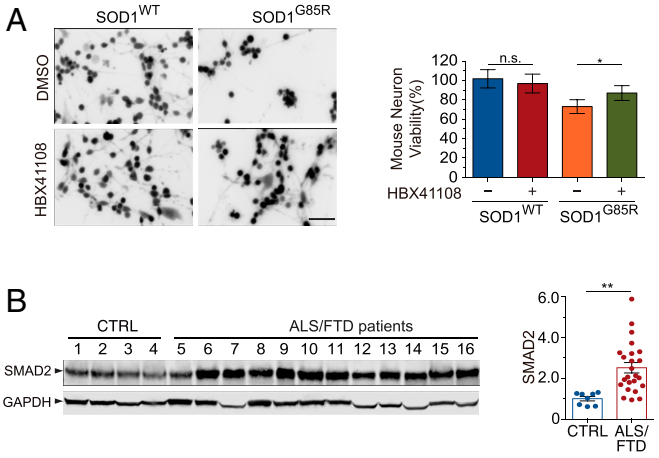


**Fig. 7.** Role of the USP7–SMAD2 pathway in neurons and patient tissues. (*A*) Mouse neurons were transduced with SOD1$^{G85R}$ or SOD1$^{WT}$ HSVs and treated with vehicle (DMSO) or the USP7 inhibitor HBX41108. (Scale bar, 150 μm.) Live cells were loaded with the calcein AM dye to determine cell viability (*Left*). Quantification of the cell viability (*Right*; $n = 8$; n.s., nonsignificant; $^{*}P < 0.05$). (*B*) Representative Western blotting of human spinal cord tissue lysates derived from ALS patients and controls show up-regulation of SMAD2 in the patients' tissues (*Left*). Quantification of the SMAD2 protein levels (*Right*; $n = 8$ for control and $n = 24$ for ALS; $^{**}P < 0.01$). Error bars indicate ± SEM.

ALS patients. Among these 24 ALS patients, 14 were documented harboring the TDP-43 proteinaceous inclusion pathology and 1 carrying the SOD1 L145F mutation (Fig. 7*B* and *SI Appendix*, Table S2). These results indicate that the SMAD2-mediated signaling pathway is dysregulated in the relevant patients' tissues.

## Discussion

The regulation of proteotoxicity likely involves complex cellular networks of which our understanding remains limited. Here we identified USP7 as a regulatory switch that significantly influences the clearance of misfolded proteins such as mutant SOD1 and TDP-43. Loss of USP7 enhances the degradation of misfolded proteins, and this action is mediated by the TGFβ–SMAD pathway, whose activation promotes protein quality control. USP7 achieves this regulation by deubiquitinating NEDD4L, which functions as an E3 ubiquitin ligase and promotes the degradation of SMAD2 (*SI Appendix*, Fig. S8). Altogether, our unbiased screening approach has identified the deubiquitinase USP7 as a strong suppressor of proteotoxicity, and our studies of downstream effectors reveal a pathway that robustly boosts protein quality control to counter the toxicity of disease-associated misfolded proteins.

USP7 and its orthologs have been implicated in the regulation of a wide range of cellular processes, including cell polarity (28) and insulin/insulin-like growth factor 1 signaling (40, 41). The present study identifies a function of USP7 as a positive regulator of proteotoxicity that is conserved in *C. elegans*, *Drosophila*, and mammalian cells. The activity of USP7 in proteotoxicity is not limited to a single protein but is potentially applicable to a variety of targets, as shown by its effects on at least two distinct types of proteins: SOD1, a well-structured enzyme, and TDP-43, an RNA-binding protein with complex domains. This effect of USP7 is mediated by a previously unknown USP7–NEDD4L–SMAD2 axis that influences protein quality control. These results reveal a layer of regulation of protein quality control and demonstrate a role for the deubiquitinase USP7 in high-level control of protein homeostasis. This role is distinct from previously reported roles of deubiquitinases in protein quality control,

which involve the direct modification of the ubiquitin chains of target proteins or core machineries for protein quality control such as proteasomes (24, 25). Here, we found that USP7 deubiquitinates the E3 ubiquitin ligase NEDD4L, which promotes the degradation of SMAD2 as a transcriptional switch for genes involved in protein quality control. Thus, USP7 is a regulator that contributes to the higher-order regulation of the cell's protein quality-control systems.

To date, our independent screens using mutant SOD1 *C. elegans* models have identified several suppressors of proteotoxicity, including UBE4B and LSD1 (18), L3MBTL1 (19), and USP7. Further studies have revealed a common theme shared by these regulators of proteotoxicity: They all modulate posttranslational modifications of transcription factors that control the expression of genes in protein quality control and thereby influence the degradation and clearance of misfolded proteins (18, 19). A signaling hub in this regulatory network appears to be the transcription factor p53 (18, 19); interestingly, USP7 has well-established roles in deubiquitinating p53 and its E3 ligase Hdm2 (42), suggesting that USP7 is part of the protein quality-control network. In the present study, we demonstrate that, in an analogous pathway, USP7 deubiquitinates the E3 ligase of SMAD2, which in turn regulates autophagy and protein quality control. We propose that SMAD2 is another signaling hub that integrates regulatory inputs to regulate the transcriptional program of protein quality control. Autophagy is critical for neuronal health and dysregulation of autophagy is a common theme for neurodegenerative diseases including ALS (43–45). Moreover, consistent with the reports that SOD1 and TDP-43 can be degraded by autophagy (46, 47), we found that the USP7–SMAD2 pathway positively regulates autophagy and thereby promotes the turnover of the ALS-associated proteins. In addition, we found that the SMAD2 protein level is up-regulated in ALS patients' tissues from the central nervous system. Together with the reports that TGFβ ligands were dysregulated in ALS patients' tissues (48), our findings suggest that the SMAD2-related protein quality-control network is implicated in ALS-associated neurodegeneration. Given that TGFβ ligands have been reported to show protective activity in mammalian models of Alzheimer's and Parkinson's diseases (49–51), it is possible that the SMAD2-related protein quality-control network is widely implicated in the pathogenesis of proteotoxicity-associated neurodegeneration and that modulating the functions of this network may be explored to as a therapeutic strategy for a broad spectrum of relevant diseases.

## Materials and Methods

**DNA Plasmids.** For mammalian expression, $SOD1^{WT}$ and $SOD1^{G85R}$ were cloned into the pEF-BOS vector, and TDP-$43^{WT}$ and TDP-$43^{Q331K}$ were cloned into the pRK5-Myc vector, as previously described (9, 15). A Gateway Donor vector encoding human NEDD4L was purchased from the Johns Hopkins Genomic Resources DNA repository (BC032597.1) and recombined in the Destination vector pDEST40 containing a V5 tag. Both pCI-Flag-USP7 and SBE4-Luc plasmids (Addgene 16655 and 16495) were previously described (31). The Cys223Ser mutation was introduced into the pCI-Flag-USP7 plasmid by site-directed mutagenesis using primer-encoded nucleotide replacements and the HiFi Assembly kit (NEB). The control Flag-GUS plasmid expressing β-glucuronidase was previously described (19). The HA-ubiquitin–expressing plasmid was purchased from Addgene (18712). The plasmids expressing USP7 shRNAs with a red fluorescent protein (RFP) marker (pRFP-C-RS, catalog no. TF308454) and the scrambled control (catalog no. TR30015) were from OriGene Technologies Inc. The SMAD2 shRNA sequence (5′-CATGATCCAGTATCACAGTAT-3′) was cloned into an L4R1-H1-promoter plasmid and used with a scrambled shRNA control as described previously (18).

***C. elegans* Strains and Assays.** *C. elegans* strains obtained from *Caenorhabditis* Genetics Center were the following: RB2194 [*math-33(ok2974)*], GR1373 [*eri-1(mg366)*], and MT2495 [*lin-15B(n744)*]. The transgenic strains in this study were the following: IW8 [*Psnb-1::SOD1$^{G85R}$-YFP(iwIs8)*] and IW31 [*Psnb-1::SOD1$^{WT}$-YFP(iwI27)*]. N2 Bristol *C. elegans* strains, cultured under standard conditions at 20 °C, were used for all experiments. The RNAi screen using the $SOD1^{G85R}$-YFP transgenic *C. elegans* with the *eri-1(mg366);lin-15B(n744)* background was described previously (26). In brief, worms at mixed stages were screened in 96-well plates in liquid medium containing individual clones of *E. coli* containing dsRNAs targeting >16,000 genes in *C. elegans*. The *math-33* suppressor hit was validated on regular nematode growth media (NGM) plates containing the specific dsRNA-expressing *E. coli*. For the thrashing assay to quantify locomotor ability, *C. elegans* was transferred into M9 buffer (3 mg/mL $KH_2PO_4$, 6 mg/mL $Na_2HPO_4$, 5 mg/mL NaCl, and 1 mM $MgSO_4$), and after 15 s of adaptation the number of body bends or thrashes was counted for 1 min as an index of the locomotor phenotype. A thrash was counted when both the head and the tail bent away from the anteroposterior axis by more than 45°. For the offspring assay, L4 larvae were grown separately on NGM plates to adulthood, and the surviving F1 larvae were counted. For the lifespan assay, synchronized eggs were transferred to new NGM plates, and the hatched *C. elegans* were followed for lifespan analysis.

***Drosophila* Strains and Assays.** *Drosophila* transgenic strains were obtained from the Bloomington or Vienna Stock Centers. Flies were maintained and crossed on standard yeast–agar–cornmeal medium at 25 °C. The *Drosophila* transgenic strain carrying *GAL4*-inducible human TDP-$43^{M337V}$ (*P{UAS-TDP-43.M337V.Myc}*) or $SOD1^{A4V}$ (*P{UAS-hSOD1.A4V}*) was recombined with *GMR-GAL4*, which drives expression in developing eyes, or *D42-GAL4* (*w*;P{w$^{+mW.hs}$ = GawB}D42*), which drives expression in motor neurons, respectively, as previously described (36, 38). The *GMR-GAL4, hTDP-43$^{M337V}$/Cyo* and *D42-GAL4, hSOD1$^{A4V}$/TM3* fly strains were crossed to the following RNAi transgenic strains: Luc (RNAi control) (*y$^1$ v$^1$; P{TRiP.JF01355}attP2*), Usp7 (*y$^1$sc*v$^1$; P{y[+t7.7]v[+t1.8]=TRiP.HMS01187}attP2*), Smox (*y$^1$ v$^1$; P{TRiP.JF02320}attP2/TM3* and *y$^1$sc*v$^1$ sev$^{21}$; P{y[+t7.7]v[+t1.8]=TRiP.HMS02203}attP40*), and Babo (*y$^1$ v$^1$; P{TRiP.HMS02033}attP40* and *w$^{1118}$; P{GD51}v853*). For the climbing assay, F1 progeny were transferred to freshly made food every 2 to 3 d during the 30-d aging period. For this assay, *Drosophila* were transferred to new empty vials, and the number of flies that could climb from the bottom to the top half of the vials during a 1-min interval was quantified. For the eye morphology and pigmentation assay, flies were aged for 7 d and then the eye morphology was examined. Changes in ommatidial structure and glossiness phenotypes were monitored for enhancement or suppression. The pigment content was measured at 488 nm and background-corrected at 600 nm using fly head protein extracts derived from two females and two males. For histological analysis of *Drosophila* eyes, flies were aged for 7 d and freshly embedded in optimal cutting temperature compound, then the eyes were cryosectioned in the thickness of 30 μm with a CryStar NX70 cryostat (Thermo Fisher). The tissue sections were air-dried, fixed with 95% ethanol, and then subjected to H&E staining analysis (H-3503; Vector Laboratories).

Deletion alleles in the *Drosophila* Usp7 gene were generated by crossing the line expressing Cas9 (*y$^1$ sc* v$^1$ sev$^{21}$; P{y$^{+t7.7}$ v$^{+t1.8}$ = nos-Cas9.R}attP40*) with the line expressing Usp7 cognate sgRNA (*y$^1$ v$^1$; P{y$^{+t7.7}$ v$^{+t1.8}$ = TKO.GS04695}attP40*). Resulting F1 male progeny were crossed en masse to X-chromosome balancer flies FM7c, 2xTb-RFP. Individual F2 females with potential Usp7 indels were crossed to FM7c, 2xTb-RFP males to establish individual lines, and the lethality of homozygous indels was assessed. Selected mutant alleles were analyzed by PCR and subsequent sequencing.

**Mammalian Cell Lines, Transfections, and Drug Treatments.** HEK293 cells were grown at 37 °C/5% $CO_2$ in standard Dulbecco's modified Eagle's medium (DMEM) supplemented with 10% fetal bovine serum (FBS). Transfections of mammalian cells were performed using Lipofectamine 2000 (Invitrogen) according to the manufacturer's recommendations. For shRNA studies, transfections of HEK293 cells were performed by plating $3.2 \times 10^5$ cells in 60-mm poly(ethyleneimine) (10 μg/mL in PBS; Sigma)-pretreated dishes 1 d before the transfection. For DNA transfections, 4 μg of shRNA-encoding plasmid, 300 ng of SOD1 reporter plasmid (pEF-BOS-$SOD1^{G85R}$), and 8 μL of Lipofectamine 2000 (Invitrogen) were mixed in 500 μL Opti-MEM I (Invitrogen) and applied to cells in 2.5 mL Opti-MEM I. At 6 h posttransfection, the medium was replaced with DMEM/10% FBS. The cells were lysed for analysis 48 to 72 h after the start of the transfections. In the USP7 inhibition studies, HEK293 cells were treated for 24 h with the drug HBX41108 at concentrations from 2 μM to 8 μM, starting at 6 h posttransfection. In the cycloheximide chase assay, cells were treated with cycloheximide at the concentration of 200 μg/mL and incubated for 0, 4, 8, and 22 h.

**mES Cells, Neuronal Differentiation, and Survival Assays.** mES cells were cultured at 37 °C/5% $CO_2$ in "2i" medium (Neurobasal, DMEM/F12, N-2 supplement, B-27 supplement, bovine albumin fraction V, PEN/STREP, PD03259010, CHIR99021, glutamine, monothioglycerol, and leukemia inhibitory factor). For differentiation of the mES cells, the cells ($1 \times 10^6$) were cultured in suspension in DFK5 medium (DMEM/F12-based medium containing 5% knockout serum replacement, 1 × insulin transferrin selenium [Thermo Fisher], 50 μM nonessential amino acids, 100 μM β-mercaptoethanol, 5 μM thymidine, 15 μM adenosine, 15 μM cytosine, 15 μM guanosine, and 15 μM uridine) for 2 d (52). They were then cultured with 2 μM retinoic acid and 600 nM smoothened agonist in fresh DFK5 medium for 4 d. The medium was replaced every other day. Finally, the ES cells were separated as single cells and plated on poly-L-ornithine– and laminin-coated 12-well plates in DFK5 medium containing 5 ng/mL glial-derived neurotrophic factor (GDNF; Peprotech), 5 ng/mL brain-derived neurotrophic factor (BDNF; Peprotech), and 5 ng/mL neurotrophin-3 (NT-3; Peprotech). After 24 h, the medium was switched to DFKNB medium supplemented with half DFK5 medium and half Neurobasal medium with 1 × B27, 5 ng/mL GDNF, 5 ng/mL BDNF, and 5 ng/mL NT-3 (52). Before changing to the DFKNB medium, the differentiated mES cells were transduced with HSV, in the presence of 4 μg/mL of polybrene, expressing $SOD1^{WT}$ or $SOD1^{G85R}$ mutant for 6 h. Three days after the HBX41108 treatment, the cells were subjected to a cell survival assay: Live neurons were rinsed twice with PBS containing calcium and magnesium then incubated with 1 μM calcein AM for 1 h at 37 °C, followed by measurement of the fluorescent signal with a plate reader (Synergy H1; BioTek).

**Western Blotting and Antibodies.** Samples were extracted in cold RIPA solution (50 mM Tris·HCl, pH 7.6, 150 mM NaCl, 1% Nonidet P-40, 1% SDS, 100 mM sodium fluoride, 17.5 mM β-glycerophosphate, 0.5% sodium deoxycholate, and 10% glycerol). The RIPA buffer was supplemented with EDTA-free protease inhibitor mixture (Roche). Lysates were placed on ice, pulse-sonicated for 10 min, and centrifuged at 10,600 × *g* at 4 °C for 10 min. The protein content in each sample was determined by a bicinchoninic acid assay (Thermo Fisher). For immunoblotting, equal amounts of proteins were electrophoresed on 15% or 4 to 20% Tris·HCl gels (Bio-Rad). Proteins were transferred to nitrocellulose membranes and immunoprobed with the following antibodies: anti-SOD1 antibodies (ADI-SOD-100; Enzo Life), anti-YFP (632381; Clontech), anti-USP7 (sc-137008; Santa Cruz), anti-GAPDH (glyceraldehyde-3-phosphate dehydrogenase) (AM4300; Thermo Scientific), anti-actin (sc-47778; Santa Cruz), anti-SMAD2/3 (8685; Cell Signaling), anti-SMAD2 (5339; Cell Signaling), anti-NEDD4L (4013; Cell Signaling), anti-HA (H6908; Sigma), anti-Flag (F3165; Sigma), anti-V5 (R960-25; Thermo Scientific), and anti-LC3 (3868; Cell Signaling).

**Immunoprecipitation.** HEK293 cells were grown in 10-cm dishes and transfected with specific plasmids by using Lipofectamine 2000. After transfection, the cells were maintained in DMEM containing 10% FBS for 48 h. Cells were extracted in cold lysis buffer (50 mM Tris·HCl, pH 7.5, with 150 mM NaCl, 0.5% sodium deoxycholate, 1% Nonidet P-40, and 1 mM EDTA) containing a protease inhibitor mixture (Roche). Cell lysates were sonicated for 5 min and centrifuged at 12,000 × *g* for 10 min at 4 °C and the supernatants collected. The cell lysates were incubated with anti-Flag (F3165; Sigma) or anti-V5 (R960-25; Thermo Scientific) antibody overnight at 4 °C and then immunoprecipitated with protein A/G magnetic beads at 4 °C for 2 h. After incubation, the beads were washed three times with cell lysis buffer then eluted with low-pH elution buffer at room temperature for 10 min. The eluents were neutralized with 1 M Tris·HCl (pH 8.0) and analyzed by immunoblotting.

**Protein Solubility Assays.** The protein solubility assay for mammalian cells and *C. elegans* was modified from previously described procedures (9, 26). HEK293 cells were grown on 60-mm plates and transfected. After 72 h, they were washed twice with cold 1× PBS and lysed in 200 μL of lysis buffer (50 mM Tris·HCl, pH 8.0, with 1 mM ethylenediaminetetraacetic acid [EDTA], 100 mM NaCl, and 0.5% Nonidet P-40, 1:200 diluted protease inhibitor mixture [P8340; Sigma], and 25 mM iodoacetamide [I6125; Sigma]). The lysates were sonicated on ice for 5 min using a Diagenode Bioruptor (high power, 30-s pulse, 30-s pause) then centrifuged for 5 min at 25 psi (~130,000 × *g*) in an Airfuge (Coulter-Beckman) to separate larger aggregates (P1) from smaller aggregates and soluble proteins (S1). The P1 pellets were washed by resuspension in lysis buffer as described above, sonicated for 5 min on ice, and centrifuged (Airfuge, ~130,000 × *g*, 5 min). The resulting pellets (P2) were resuspended in 50 μL urea/SDS buffer (8 M urea, 5% SDS; 40 mM Tris·HCl, pH 6.8, and 0.1 mM EDTA) and sonicated for 5 min to solubilize the aggregates. The S1 and P2 fractions were analyzed by SDS/PAGE and immunoblotting. Actin or GAPDH in the soluble S1 fraction was used as a loading control. *C. elegans* were harvested from NGM plates by washing with M9 buffer five times. After washing, the worm pellets were lysed in the lysis buffer and fractioned into S1 and P2 pellets as described above.

**Transcriptional Activity Luciferase Assay.** Cells were transfected with the firefly luciferase SMAD reporter plasmid containing the SMAD-binding consensus sequence (31), together with a thymidine kinase promoter *Renilla* luciferase (tk-Rluc) reporter for normalization. At 24 h posttransfection, the cells were lysed in passive lysis buffer (Promega) and analyzed with the Dual-Luciferase Reporter System according to the manufacturer's recommendations (Promega), using an injector-equipped Synergy H1 microplate reader (BioTek).

**qRT-qPCR.** Total RNA was isolated from *C. elegans* or *Drosophila* larvae by using the RNeasy Plus Mini kit (Qiagen). For quantitative RT-qPCR, cDNAs were synthesized with the QuantiTect reverse transcription kit (Qiagen) using the RNA samples. Primers for quantitative RT-qPCR were as follows: human SOD1 (forward [F]: 5′GGGAAGCTGTTGTCCCAAG3′; reverse [R]: 5′CAAGGGGAGGTAAAAGAGAGC3′). *Drosophila* Usp7 (F: 5′AGGACACCCAAGAGGTCGAG3′; R: 5′ATCGGCCAATAGTTGTTGTGG3′); *Drosophila* Smox (F: 5′GGCCCGATCTCCAGAGTC3′; R: 5′CACCAGGATGGACAGTTCAATTT3′); *Drosophila* Babo (F: 5′GCGAAAAAGCCAGAAAACA3′; R: 5′CATATATTGTTCGATTCCTTGCAC3′). RT-qPCRs were performed on a Bio-Rad thermal cycler with the PowerUp SYBR Green master mix (Thermo Fisher).

**Microarray Transcriptional Profiling.** Total RNA was isolated from HEK293 cells with the RNeasy Mini kit and analyzed using the Affymetrix human GENE 1.0ST array. The microarray data were managed using the Partek Genomic Suite (Partek Inc.) and Spotfire DecisionSite software (TIBCO Software Inc.) and analyzed using Ingenuity Pathways Analysis software (IPA, Ingenuity Systems). In addition to RNA, total protein was isolated from the same samples by acetone precipitation to verify the reduction in the USP7 protein level.

The network analysis and upstream regulator analysis were performed using the IPA software. The molecules with expression fold changes above the threshold were overlaid onto a global molecular network developed from information contained in the Ingenuity Knowledge Base. The probability of a significant overlap between microarray-derived and literature-derived sets was set to $<0.05$. The significant agreement between the literature-predicted versus microarray-derived activation/inhibition states of an upstream regulator, or the z-score, was set to $\geq 2.0$. The raw data from the present microarray analysis are deposited at the Gene Expression Omnibus (GEO) repository (accession no. GSE139094).

**Deubiquitination Assays In Vitro and In Vivo.** For the in vitro deubiquitination assay, HEK293 cells were cultured in 10-cm dishes and transfected with plasmids expressing V5-NEDD4L and HA-Ub. After 48 h of transfection, cells were lysed in lysis buffer (0.5% sodium deoxycholate, 50 mM Tris·HCl, pH 7.5, 150 mM NaCl, 1% Nonidet P-40, 1 mM EDTA, pH 8.0, and and protease inhibitors) and immunoprecipitated with anti-V5 antibody. The ubiquitinated V5-NEDD4L protein (bound to the G protein-coupled anti-V5 antibody) was used as a substrate in the in vitro deubiquitination assays (53, 54) as follows. Ubiquitinated V5-NEDD4L was incubated with GST or GST-USP7 (Sino Biological) in deubiquitination buffer (50 mM Tris·HCl, pH 8.0, 50 mM NaCl, 1 mM EDTA, pH 8.0, 10 mM dithiothreitol, and 5% glycerol) at 37 °C for 2 h. The beads were washed three times with washing buffer (50 mM Tris·HCl, pH 8.0, 150 mM NaCl, and 0.4% Nonidet P-40) then eluted with low-pH elution buffer at room temperature for 10 min. The eluents were neutralized with 1 M Tris·HCl (pH 8.0) and analyzed by immunoblotting.

For the in vivo deubiquitination assay, HEK293 cells were cultured in 10-cm dishes and transfected with plasmids expressing V5-NEDD4L, HA-Ub, and Flag-USP7, Flag-$USP7^{C223S}$, or Flag-GUS. After 48 h of transfection, the cells were lysed in lysis buffer (0.5% sodium deoxycholate, 50 mM Tris·HCl, pH 7.5, 150 mM NaCl, 1% Nonidet P-40, 1 mM EDTA, pH 8.0, protease inhibitors, and 10 mM *N*-ethylmaleimide). The lysates were incubated with anti-V5 antibody to pull down NEDD4L, and the immunoprecipitates were eluted and analyzed by immunoblotting.

**Proteasome Activity Assay.** HEK293 cells were cultured in 6-cm dishes and transfected with shRNA control or shRNA against SMAD2. After 72 h, transfected cells were split into white-walled 96-well plates at a density of 5,000 cells per well. After 4 h, the proteasome activity assay was performed by using the proteasome-Glo Cell-Based kit (G8660; Promega), and luminescence was measured by using an injector-equipped Synergy H1 microplate reader (BioTek).

**Immunofluorescence.** HEK293 cells were seeded on coated coverslips. The next day, the cells were transfected with a plasmid expressing mCherry-EGFP-LC3 (pDest-mCherry-EGFP-LC3) (55). After 2 d, cells were fixed with 4% paraformaldehyde solution in PBS for 15 min, followed by washing with PBS for 10 min three times. The coverslips were mounted with ProLong Gold Antifade Mountant (Thermo Fisher). Images were collected with a Leica SP8 laser scanning confocal microscope.

**Human Tissues.** Frozen human postmortem spinal cords were sectioned and weighed and then lysed in a weight (milligrams):volume (microliters) ratio of 1:10 using cold lysis buffer containing 50 mM Tris·HCl, pH7.5, 150 mM NaCl, 1% Nonidet P-40, 0.1% SDS, 100 mM NaF, 17.5 mM β-glycerophosphate, 0.5% sodium deoxycholate, 10% glycerol, 1 mM phenylmethylsulfonyl fluoride, 2 mM $Na_3VO_4$, protease inhibitors, and phosphatase inhibitor mixture 2/3. The lysates were probe-sonicated on ice for 5 min twice and centrifuged at 12,000 × *g* for 15 min at 4 °C, and the supernatants were collected. The tissue lysates were analyzed by SDS-PAGE and immunoblotting. Postmortem spinal cord tissues used in this study are described in *SI Appendix*, Table S2.

**Bioinformatic and Statistical Analysis.** The phylogenetic tree analysis was performed using the tools on the Phylogeny.fr web site (MUSCLE for alignment of protein sequences, Gblocks for curation, and PhyML for tree building) (56). The resulting output in the Newick file format was fed into EvolView for the graphical tree output (57).

All quantification and statistical tests were performed using GraphPad Prism software (Version 7.0). The *P* values for all experiments were obtained using unpaired Student's *t* tests unless otherwise indicated.

**Data Availability.** Microarray transcriptional profiling data have been deposited in the Gene Expression Omnibus (accession no. GSE139094).

**ACKNOWLEDGMENTS.** We thank Arthur Horwich for support and Krystyna Furtak for technical assistance during the initial *C. elegans* screen, Bert Vogelstein for USP7 and SBE4 reporter constructs, Terje Johansen for the mCherry-EGFP-LC3 construct, and other J.W. laboratory members for technical assistance and discussions. Several strains were obtained from the *Caenorhabditis* Genetic Center, which was funded by NIH Office of Research Infrastructure Programs (P40 OD010440). This work was supported by grants from the NIH (NS074324, NS089616, and NS110098), Packard Center for ALS Research at Johns Hopkins, Muscular Dystrophy Association, the US Department of Defense, and the ALS Association to J.W.

1. B. Bukau, A. L. Horwich, The Hsp70 and Hsp60 chaperone machines. *Cell* **92**, 351–366 (1998).
2. A. Ciechanover, P. Brundin, The ubiquitin proteasome system in neurodegenerative diseases: Sometimes the chicken, sometimes the egg. *Neuron* **40**, 427–446 (2003).
3. E. Wong, A. M. Cuervo, Autophagy gone awry in neurodegenerative diseases. *Nat. Neurosci.* **13**, 805–811 (2010).
4. S. B. Prusiner, Cell biology. A unifying role for prions in neurodegenerative diseases. *Science* **336**, 1511–1513 (2012).
5. W. E. Balch, R. I. Morimoto, A. Dillin, J. W. Kelly, Adapting proteostasis for disease intervention. *Science* **319**, 916–919 (2008).
6. D. W. Cleveland, J. D. Rothstein, From Charcot to Lou Gehrig: Deciphering selective motor neuron death in ALS. *Nat. Rev. Neurosci.* **2**, 806–819 (2001).
7. D. R. Rosen *et al*., Mutations in Cu/Zn superoxide dismutase gene are associated with familial amyotrophic lateral sclerosis. *Nature* **362**, 59–62 (1993).
8. J. S. Valentine, P. J. Hart, Misfolded CuZnSOD and amyotrophic lateral sclerosis. *Proc. Natl. Acad. Sci. U.S.A.* **100**, 3617–3622 (2003).
9. J. Wang *et al*., Copper-binding-site-null SOD1 causes ALS in transgenic mice: Aggregates of non-native SOD1 delineate a common feature. *Hum. Mol. Genet.* **12**, 2753–2764 (2003).
10. H.-X. Deng *et al*., Amyotrophic lateral sclerosis and structural defects in Cu,Zn superoxide dismutase. *Science* **261**, 1047–1051 (1993).
11. Y. Zhong *et al*., Nuclear export of misfolded SOD1 mediated by a normally buried NES-like sequence reduces proteotoxicity in the nucleus. *eLife* **6**, e23759 (2017).
12. A. E. Renton, A. Chiò, B. J. Traynor, State of play in amyotrophic lateral sclerosis genetics. *Nat. Neurosci.* **17**, 17–23 (2014).
13. M. Neumann *et al*., Ubiquitinated TDP-43 in frontotemporal lobar degeneration and amyotrophic lateral sclerosis. *Science* **314**, 130–133 (2006).
14. K. A. Josephs *et al*., TDP-43 is a key player in the clinical features associated with Alzheimer's disease. *Acta Neuropathol.* **127**, 811–824 (2014).
15. T. Zhang, P. C. Mullane, G. Periz, J. Wang, TDP-43 neurotoxicity and protein aggregation modulated by heat shock factor and insulin/IGF-1 signaling. *Hum. Mol. Genet.* **20**, 1952–1965 (2011).
16. E. L. Guenther *et al*., Atomic structures of TDP-43 LCD segments and insights into reversible or pathogenic aggregation. *Nat. Struct. Mol. Biol.* **25**, 463–471 (2018).
17. J. Zou, Y. Guo, T. Guettouche, D. F. Smith, R. Voellmy, Repression of heat shock transcription factor HSF1 activation by HSP90 (HSP90 complex) that forms a stress-sensitive complex with HSF1. *Cell* **94**, 471–480 (1998).
18. G. Periz *et al*., Regulation of protein quality control by UBE4B and LSD1 through p53-mediated transcription. *PLoS Biol.* **13**, e1002114 (2015).
19. J. Lu *et al*., L3MBTL1 regulates ALS/FTD-associated proteotoxicity and quality control. *Nat. Neurosci.* **22**, 875–886 (2019).
20. Y. Miyazaki, L. C. Chen, B. W. Chu, T. Swigut, T. J. Wandless, Distinct transcriptional responses elicited by unfolded nuclear or cytoplasmic protein in mammalian cells. *eLife* **4**, e07687 (2015).
21. Y. T. Kwon, A. Ciechanover, The ubiquitin code in the ubiquitin-proteasome system and autophagy. *Trends Biochem. Sci.* **42**, 873–886 (2017).
22. C. M. Pickart, Mechanisms underlying ubiquitination. *Annu. Rev. Biochem.* **70**, 503–533 (2001).
23. M. J. Clague, S. Urbé, D. Komander, Breaking the chains: Deubiquitylating enzyme specificity begets function. *Nat. Rev. Mol. Cell Biol.* **20**, 338–352 (2019).
24. J. Hanna *et al*., Deubiquitinating enzyme Ubp6 functions noncatalytically to delay proteasomal degradation. *Cell* **127**, 99–111 (2006).
25. B. H. Lee *et al*., USP14 deubiquitinates proteasome-bound substrates that are ubiquitinated at multiple sites. *Nature* **532**, 398–401 (2016).
26. J. Wang *et al*., An ALS-linked mutant SOD1 produces a locomotor defect associated with aggregation and synaptic dysfunction when expressed in neurons of Caenorhabditis elegans. *PLoS Genet.* **5**, e1000350 (2009).
27. R. S. Kamath *et al*., Systematic functional analysis of the Caenorhabditis elegans genome using RNAi. *Nature* **421**, 231–237 (2003).
28. R. J. McCloskey, K. J. Kemphues, Deubiquitylation machinery is required for embryonic polarity in Caenorhabditis elegans. *PLoS Genet.* **8**, e1003092 (2012).
29. J. Wang, G. Xu, D. R. Borchelt, High molecular weight complexes of mutant superoxide dismutase 1: Age-dependent and tissue-specific accumulation. *Neurobiol. Dis.* **9**, 139–148 (2002).
30. F. Colland *et al*., Small-molecule inhibitor of USP7/HAUSP ubiquitin protease stabilizes and activates p53 in cells. *Mol. Cancer Ther.* **8**, 2286–2295 (2009).
31. L. Zawel *et al*., Human Smad3 and Smad4 are sequence-specific transcription activators. *Mol. Cell* **1**, 611–617 (1998).
32. S. Gao *et al*., Ubiquitin ligase Nedd4L targets activated Smad2/3 to limit TGF-beta signaling. *Mol. Cell* **36**, 457–468 (2009).
33. M. Li *et al*., Deubiquitination of p53 by HAUSP is an important pathway for p53 stabilization. *Nature* **416**, 648–653 (2002).
34. L. Tadlock, Y. Yamagiwa, J. Hawker, C. Marienfeld, T. Patel, Transforming growth factor-beta inhibition of proteasomal activity: A potential mechanism of growth arrest. *Am. J. Physiol. Cell Physiol.* **285**, C277–C285 (2003).
35. K. Kiyono *et al*., Autophagy is activated by TGF-beta and potentiates TGF-beta-mediated growth inhibition in human hepatocellular carcinoma cells. *Cancer Res.* **69**, 8844–8852 (2009).
36. M. R. Watson, R. D. Lagow, K. Xu, B. Zhang, N. M. Bonini, A drosophila model for amyotrophic lateral sclerosis reveals motor neuron damage by human SOD1. *J. Biol. Chem.* **283**, 24972–24981 (2008).
37. T. Brummel *et al*., The Drosophila activin receptor baboon signals through dSmad2 and controls cell proliferation but not patterning during larval development. *Genes Dev.* **13**, 98–111 (1999).
38. G. P. Ritson *et al*., TDP-43 mediates degeneration in a novel Drosophila model of disease caused by mutations in VCP/p97. *J. Neurosci.* **30**, 7729–7739 (2010).
39. M. L. Schlief, T. West, A. M. Craig, D. M. Holtzman, J. D. Gitlin, Role of the Menkes copper-transporting ATPase in NMDA receptor-mediated neuronal toxicity. *Proc. Natl. Acad. Sci. U.S.A.* **103**, 14919–14924 (2006).
40. T. Heimbucher *et al*., The deubiquitylase MATH-33 controls DAF-16 stability and function in metabolism and longevity. *Cell Metab.* **22**, 151–163 (2015).
41. M. M. Senchuk *et al*., Activation of DAF-16/FOXO by reactive oxygen species contributes to longevity in long-lived mitochondrial mutants in Caenorhabditis elegans. *PLoS Genet.* **14**, e1007268 (2018).
42. O. Tavana, W. Gu, Modulation of the p53/MDM2 interplay by HAUSP inhibitors. *J. Mol. Cell Biol.* **9**, 45–52 (2017).

43. A. Yamamoto, Z. Yue, Autophagy and its normal and pathogenic states in the brain. *Annu. Rev. Neurosci.* **37**, 55–78 (2014).
44. R. A. Nixon, The role of autophagy in neurodegenerative disease. *Nat. Med.* **19**, 983–997 (2013).
45. D. K. H. Nguyen, R. Thombre, J. Wang, Autophagy as a common pathway in amyotrophic lateral sclerosis. *Neurosci. Lett.* **697**, 34–48 (2019).
46. J. Gal *et al*., Sequestosome 1/p62 links familial ALS mutant SOD1 to LC3 via an ubiquitin-independent mechanism. *J. Neurochem.* **111**, 1062–1073 (2009).
47. S. J. Barmada *et al*., Autophagy induction enhances TDP43 turnover and survival in neuronal ALS models. *Nat. Chem. Biol.* **10**, 677–685 (2014).
48. S. Peters *et al*., The TGF-β system as a potential pathogenic player in disease modulation of amyotrophic lateral sclerosis. *Front. Neurol.* **8**, 669 (2017).
49. T. Wyss-Coray *et al*., TGF-beta1 promotes microglial amyloid-beta clearance and reduces plaque burden in transgenic mice. *Nat. Med.* **7**, 612–618 (2001).
50. I. Tesseur *et al*., Deficiency in neuronal TGF-β signaling leads to nigrostriatal degeneration and activation of TGF-β signaling protects against MPTP neurotoxicity in mice. *J. Neurosci.* **37**, 4584–4592 (2017).
51. R. von Bernhardi, F. Cornejo, G. E. Parada, J. Eugenín, Role of TGFβ signaling in the pathogenesis of Alzheimer's disease. *Front. Cell. Neurosci.* **9**, 426 (2015).
52. D. A. McCreedy *et al*., A new method for generating high purity motoneurons from mouse embryonic stem cells. *Biotechnol. Bioeng.* **111**, 2041–2055 (2014).
53. L. Jiang *et al*., Ubiquitin-specific peptidase 7 (USP7)-mediated deubiquitination of the histone deacetylase SIRT7 regulates gluconeogenesis. *J. Biol. Chem.* **292**, 13296–13311 (2017).
54. A. Dar, E. Shibata, A. Dutta, Deubiquitination of Tip60 by USP7 determines the activity of the p53-dependent apoptotic pathway. *Mol. Cell. Biol.* **33**, 3309–3320 (2013).
55. S. Pankiv *et al*., p62/SQSTM1 binds directly to Atg8/LC3 to facilitate degradation of ubiquitinated protein aggregates by autophagy. *J. Biol. Chem.* **282**, 24131–24145 (2007).
56. A. Dereeper *et al*., Phylogeny.fr: Robust phylogenetic analysis for the non-specialist. *Nucleic Acids Res.* **36**, W465–W469 (2008).
57. B. Subramanian, S. Gao, M. J. Lercher, S. Hu, W. H. Chen, Evolview v3: A webserver for visualization, annotation, and management of phylogenetic trees. *Nucleic Acids Res.* **47**, W270–W275 (2019).